OPEN

Citation: Cell Death and Disease (2014) 5, e1382; doi:10.1038/cddis.2014.348

www.nature.com/cddis

Amyloid-β induces NLRP1-dependent neuronal pyroptosis in models of Alzheimer's disease

M-S Tan[1], L Tan*[,1,2,3], T Jiang[3], X-C Zhu[3], H-F Wang[3], C-D Jia[4] and J-T Yu*[,1,2,3,5]

Increasing evidence has shown the aberrant expression of inflammasome-related proteins in Alzheimer's disease (AD) brain; these proteins, including NLRP1 inflammasome, are implicated in the execution of inflammatory response and pyroptotic death. Although current data are associated *NLRP1* genetic variants with AD, the involvement of NLRP1 inflammasome in AD pathogenesis is still unknown. Using APPswe/PS1dE9 transgenic mice, we found that cerebral NLRP1 levels were upregulated. Our *in vitro* studies further showed that increased NLRP1-mediated caspase-1-dependent 'pyroptosis' in cultured cortical neurons in response to amyloid-β. Moreover, we employed direct *in vivo* infusion of non-viral small-interfering RNA to knockdown NLRP1 or caspase-1 in APPswe/PS1dE9 brain, and discovered that these NLRP1 or caspase-1 deficiency mice resulted in significantly reduced neuronal pyroptosis and reversed cognitive impairments. Taken together, our findings indicate an important role for NLRP1/caspase-1 signaling in AD progression, and point to the modulation of NLRP1 inflammasome as a promising strategy for AD therapy.
Cell Death and Disease (2014) **5,** e1382; doi:10.1038/cddis.2014.348; published online 21 August 2014

Alzheimer's disease (AD), the most common cause of dementia, is characterized clinically by a progressive and irreversible loss of cognitive functions and pathologically by the loss of synapses and neuronal death, as well as the presence of extracellular deposits of amyloid-β (Aβ) peptides in senile plaques.[1] The main factors responsible for Aβ accumulation are disease-causing inherited variants of amyloid precursor protein (*APP*), presenilin 1 and 2 (*PS1, PS2*), or apolipoprotein E (*ApoE*) genes, and increased extracellular Aβ levels that cause neuronal death via a number of possible mechanisms including oxidative stress, excitotoxicity, energy depletion, inflammation, and apoptosis.[2,3] However, the detailed mechanisms that underlie the pathogenic nature of Aβ-induced neuronal degeneration in AD are not completely understood.

Recently, a novel inflammasome signaling pathway has been uncovered and the aberrant expression of inflammasome-related proteins have been found in AD brain and transgenic mouse models of AD.[4–6] Meanwhile, increasing evidence has supported that Aβ and misfolded protein aggregates can activate the inflammasome,[7,8] which serves as a caspase-1-activation platform for subsequent pro-inflammatory cytokine secretion and pyroptotic cell death.[9,10] In contrast to apoptosis, pyroptosis is caspase-1-mediated inflammatory cell death characterized by early plasma membrane rupture and release of pro-inflammatory intracellular contents.[11,12] Besides the neuronal loss as a prominent cause of cognitive deficits in AD, current studies have pointed out that inflammatory mechanisms are also powerful pathogenic forces in the process of neurodegeneration.[13–15]

The NLRP1 (NOD-like receptor (NLR) family, pyrin domain containing 1; previously known as NALP1) inflammasome was the first member of the NLR family to be discovered. As a critical component of the inflammasome, NLRP1 appears to be expressed rather ubiquitously, and high NLRP1 levels were also found in the brain, in particular in pyramidal neurons and oligodendrocytes.[16] It has been reported that active NLRP1 can generate a functional caspase-1-containing inflammasome *in vivo* to drive the inflammatory response and pyroptotic death.[17] Moreover, inhibition of the NLRP1 inflammasome could reduce the innate immune response and ameliorate age-related cognitive deficits in different animal models.[18–20] Although current data regarding NLRP1 functions are far scarcer than those described for other inflammasomes, various immune inflammation diseases have been associated with mutations and polymorphisms in the *NLRP1* gene. This genetic association has also been validated independently in AD patients,[21] thus indicating a potential role for the NLRP1 inflammasome in AD pathogenesis.

In this study, we first investigated whether NLRP1 expression is altered in the brains of APPswe/PS1dE9 double transgenic mice, and found an upregulated NLRP1 expression in the neurons of the brain. Meanwhile, our *in vitro* study showed that Aβ could increase NLRP1 levels in primary

[1]Department of Neurology, Qingdao Municipal Hospital, College of Medicine and Pharmaceutics, Ocean University of China, Qingdao, China; [2]Department of Neurology, Qingdao Municipal Hospital, School of Medicine, Qingdao University, Qingdao, China; [3]Department of Neurology, Qingdao Municipal Hospital, Nanjing Medical University, Qingdao, China; [4]Chemical Sciences Division, Oak Ridge National Laboratory, Oak Ridge, TN 37831, USA and [5]Department of Neurology, Memory and Aging Center, University of California, San Francisco, CA, USA

*Corresponding authors: L Tan or J-T Yu, Department of Neurology, Qingdao Municipal Hospital, School of Medicine, Qingdao University, No. 5 Donghai Middle Road, Qingdao, Shandong 266071, China. Tel: +86 186 6399 6215; Fax: +86 532 8890 5659; E-mail: dr.tanlan@163.com or Tel: +86 186 7899 9982; Fax: +86 532 8890 5659; E-mail: yu-jintai@163.com

Abbreviations: Aβ, amyloid-β; AD, Alzheimer's disease; ApoE, apolipoprotein E; APP, amyloid precursor protein; ASC, apoptosis associated speck-like protein containing a caspase recruitment domain; IL-1, interleukin 1; LDH, lactate dehydrogenase; MWM, Morris water maze; NLRP1, NOD-like receptor (NLR) family pyrin domain containing 1; PS, presenilin; siRNA, small-interfering RNA

Received 10.4.14; revised 10.7.14; accepted 21.7.14; Edited by A Verkhratsky

cortical neurons; this increase, in turn, activates caspase-1 signaling responsible for neuronal pyroptosis and inflammation-induced cytokine release, suggesting that NLRP1/caspase-1 signaling is one of the key pathways responsible for Aβ neurotoxicity. Using the pump-mediated *in vivo* infusion of non-viral small-interfering RNA (siRNA) to knockdown NLRP1 or caspase-1 in the brain of APP/PS1 mice, our study further indicated that inhibition of NLRP1 inflammasome represents a promising strategy for the development of AD therapy.

Results

NLRP1 was upregulated in the brains of APPswe/PS1dE9 mice. We first investigated whether NLRP1 expression is altered in the brains of APP/PS1 mice overexpressing the Swedish mutation of *APP* together with *PS1* deleted in exon 9. Total proteins were extracted from the cortical and hippocampal regions of 3-, 6-, and 9-month-old APP/PS1 and age-matched wild-type mice, and subjected them to western blot analysis. Compared with age-matched wild-type mice, we found that 6-month APP/PS1 mice had displayed significantly upregulated NLRP1 levels, while the levels of NeuN were slightly reduced; these shifts were more obvious in 9-month APP/PS1 mice (Figures 1a and b). Using double immunofluorescence staining to colocalize NLRP1 with neuronal marker NeuN, our result further demonstrated the increased neuronal expression of NLRP1 in the NeuN-positive neurons of APP/PS1 mice brain (Figure 1c).

$A\beta_{1-42}$ increased NLRP1 expression levels in cultured cortical neurons. In APPswe/PS1dE9 brains, the accumulation of Aβ occurs at an early stage, and amyloid deposition is visible by 6 months of age.[22] Therefore, we hypothesized that an increase in NLRP1 expression level in the brains of 6- and 9-month-old APP/PS1 mice is due to an increase in Aβ level. To test this hypothesis, we determined by western blot analysis the NLRP1 levels in cultured rat cortical neurons treated with 5 μM $A\beta_{1-42}$ for 24 h. Given that the oligomeric forms of Aβ are reportedly one of the primary neurotoxic Aβ species,[23] we prepared the toxic oligomers and confirmed their species (Supplementary Figure S1a) as described before.[24] Our study showed that NLRP1 expression was markedly increased by $A\beta_{1-42}$ in the primary cultured neurons (Supplementary Figure S1b). Next, we further measured the NLRP1 mRNA levels in these cells treated with $A\beta_{1-42}$ at an indicated dose by real-time PCR analysis. As shown in Supplementary Figure S1c, treatment with $A\beta_{1-42}$ significantly increased NLRP1 mRNA levels in a dose-dependent manner.

NLRP1-mediated Aβ-induced neurotoxicity via pyroptosis in cultured cortical neurons. Aβ causes neuronal damage via a number of possible pathways. We examined whether increased NLRP1 was involved in the process of Aβ neurotoxicity. For this purpose, we first decreased the NLRP1 levels in primary cortical neurons by NLRP1 siRNA transfection. Forty-eight hours after transfection, the cells

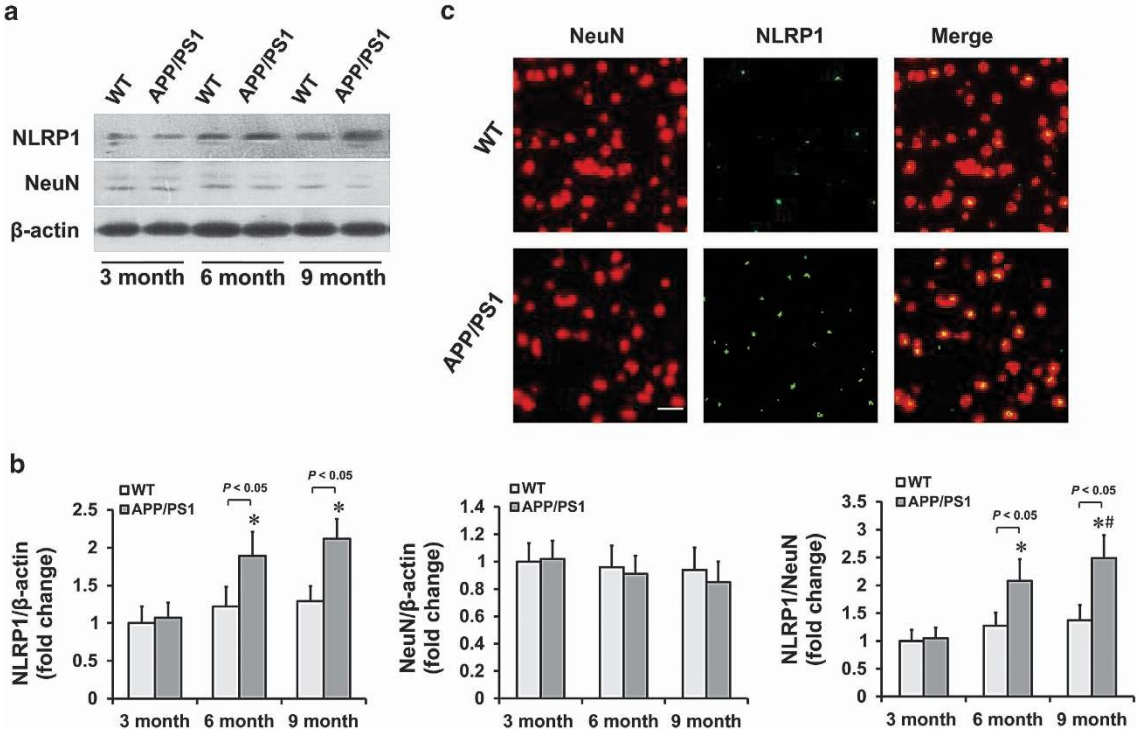

Figure 1 Increased expression of NLRP1 in the neurons of APPswe/PS1dE9 mice brain. (**a**) Cerebral NLRP1 and NeuN levels from different aged APP/PS1 and wild-type (WT) mice were detected by western blot analysis. β-actin was used as a loading control. (**b**) Levels of NLRP1, NeuN, and NLRP1/NeuN were quantified by densitometric measurement. Values are the mean ± S.E.M. $^{*}P<0.05$ *versus* 3-month-old APP/PS1 mice, $^{\#}P<0.05$ *versus* 6-month-old APP/PS1 mice. (**c**) Double immunofluorescent detection of NLRP1 in the NeuN-positive neurons of APP/PS1 mice. Tissue samples from 6-month-old APP/PS1 and WT mice were immunostained using anti-NLRP1 and anti-NeuN antibodies and examined under a fluorescence microscope. Scale bars: 20 μm. $n=6$ male mice per age group

were incubated in different doses of $A\beta_{1-42}$ for 24 h. The NLRP1 level was determined by western blot analysis. As shown in Figure 2a and Supplementary Figure S2, the transfection of NLPR1 siRNA efficiently decreased the NLRP1 levels in cultured cortical neurons. In the presence of 5 μM $A\beta_{1-42}$, siRNA-induced knockdown of NLRP1 level was very significant (by 55%). Next, we determined the effects of NLRP1 knockdown on $A\beta_{1-42}$-induced neurotoxicity. Cell viability was then assessed by MTT assay. As shown in Figure 2b, the percentage of surviving neurons was significantly increased in NLRP1 siRNA-transfeced cells compared with the control siRNA-transfected cells after the treatment with $A\beta_{1-42}$, indicating that NLRP1 at least one component for Aβ-induced neuronal death. Incidentally, the NLRP1 levels and cell viability between control siRNA-treated and No siRNA-treated cells do not differ (Figures 2a and b), excluding an effect of siRNA transfection on neuron viability.

To further investigate the possible mechanism involved in the neuron death with increased NLRP1 levels, we analyzed DNA breaks by TUNEL assay and caspase-1 activity by immunoblotting in NLRP1 siRNA- and control siRNA-transfected cells after $A\beta_{1-42}$ treatment. Our data showed in the cultured cortical neurons that the treatment of NLRP1 siRNA resulted in a significant decrease in the number of TUNEL-positive cells (Figures 2c and d), and downregulation in active caspase-1 level (Figures 2e and f) in the presence of $A\beta_{1-42}$. We further analyzed Aβ neurotoxicity by measuring secretion of the pro-inflammatory cytokine IL-1β and lactate dehydrogenase (LDH) release in the culture media of NLRP1 siRNA- and control siRNA-transfected cells. We found that knockdown of NLRP1 also markedly reduced IL-1β secretion and LDH release to the culture supernatant of the Aβ-treated neurons (Figures 2e, g, and h). Moreover, inflammasomes require the adapter protein apoptosis associated speck-like protein containing a CARD (ASC) for the activation of caspase-1;

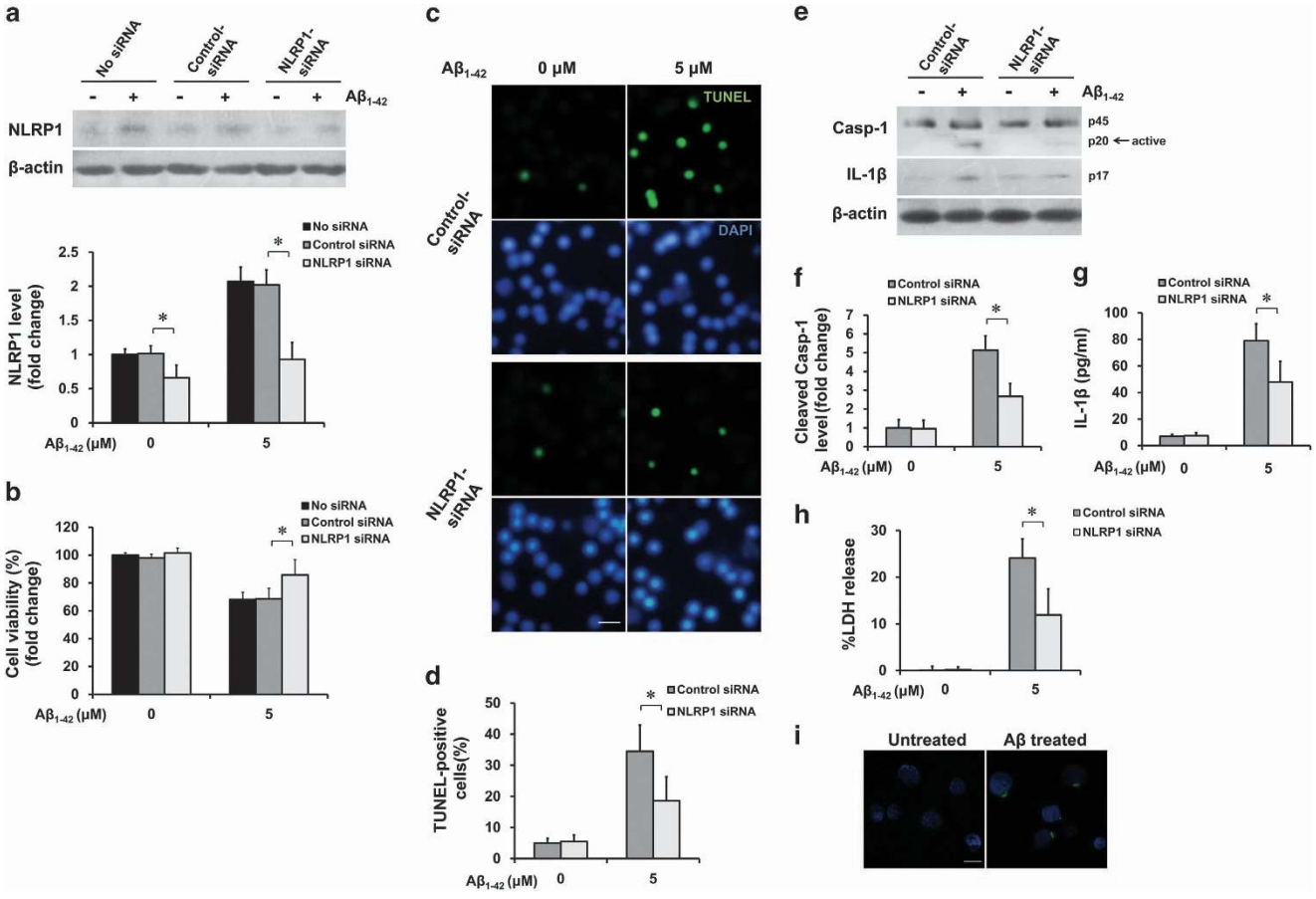

Figure 2 NLRP1 regulated pyroptosis in primary cortical neurons in the presence of Aβ. Knockdown of NLRP1 in primary cortical neurons. Primary cortical neurons were transfected with NLRP1 siRNA or control siRNA for 48 h. After transfection, the cells were then incubated in the presence or absence of 5 μM Aβ for 24 h. (**a**) The expression levels of NLRP1 were determined by western blot analysis and quantified by densitometric measurement. β-Actin was used as a loading control. (**b**) Cell viability was determined by MTT assay and shown as a percentage of surviving cells. (**c**) DNA breaks were analyzed by TUNEL assay; and cell nuclei were stained with DAPI. Representative images of DAPI-stained and TUNEL-positive cells were shown. Scale bars: 20 μm. (**d**) Quantification for the percentage of TUNEL-positive cells. (**e**) The release of caspase-1 (procaspase-1 p45 45 kD and cleaved caspase-1 p20 subunit 20 kD) and cleaved IL-1β to the culture medium was examined by immunoblotting. β-Actin was used as a loading control. (**f**) Levels of cleaved caspase-1 p20 were quantified by densitometric measurement. (**g**) The presence of IL-1β in cell culture supernatants was measured by ELISA. (**h**) The release of LDH into culture supernatants and expressed as the percentage of LDH release compared with a maximum lysis control. (**i**) Typical result of Aβ untreated and treated cells. Fluorescent microscopy images showing the bright, small speck-like, perinuclear localization of ASC foci (green) with nuclei visualized by DAPI staining (blue) in the right panel. Scale bars: 10 μm. All values are presented as the mean ± S.E.M. of three independent experiments. *$P < 0.05$ *versus* control siRNA treatment

we therefore analyzed inflammasome activation by ASC speck visualization in the presence of $A\beta_{1-42}$ (Figure 2i). Since this form of cell death is associated with caspase-1 activation in response to ASC adapter protein oligomerization, plasma membrane permeabilization, and secretion of inflammatory cytokine IL-1β, we refer to it as pyroptosis.[11,12] All these findings indicated that NLRP1 silencing may protect against Aβ neurotoxicity through caspase-1-dependent pyroptosis mechanism in cultured neurons.

NLRP1 silencing attenuated neuron pyroptosis in APPswe/PS1dE9 mice. Next, we investigate the effects of NLRP1 silencing on neuron pyroptosis in APPswe/PS1dE9 transgenic mice, a classical model of AD. Toward this end, we knocked down brain NLRP1 expression at an early stage in 5-month-old mice by using *in vivo* non-viral RNA interference methodology, which has emerged as a powerful tool to produce a widespread downregulation of target gene in the brain.[25–27] Until the end of the experiment (6.5 months of age), a time when cerebral amyloid plaques and early cognitive deficits can be observed,[22] the approach of siRNA infusion produced a significant downregulation of NLRP1 mRNA and protein levels in mice brain (Supplementary Figures S3a and b). We first determined the effects of NLRP1 knockdown on neuronal survival by Nissl staining. As shown in Figures 3a and b, the NLRP1 siRNA-treated APPswe/PS1dE9 mice showed an increase in Nissl-positive cell densities in the cortex and the hippocampus, when compared with control siRNA-treated mice. To characterize the pyroptotic effects of NLRP1, the TUNEL staining assay was used. As shown in Figures 3c and d, the number of TUNEL-positive cells in the cortex and hippocampus of APP/PS1 mice was increased and this enhancement could be inhibited by NLRP1 siRNA treatment. We further examined the changes in caspase-1, which has been known to play a central role in the execution of pyroptosis. Western blot analysis was performed at 6.5 months after the APP/PS1 mice were treated to measure the caspase-1 expression (Figure 3e). The group of APP/PS1 mice showed a robust increase in the expression of caspase-1, while the NLRP1 siRNA treatment could reduce the active caspase-1 levels in these mice.

In addition to pyroptosis, the NLRP1 inflammasome is also responsible for caspase-1-dependent processing of the key pro-inflammatory cytokine IL-1β to an active secreted form.[28,29] Previous studies have demonstrated that IL-1β is chronically upregulated in AD and believed to serve as a part of an inflammatory cycle that regulates AD pathology.[30–32] Therefore, we inspected the cerebral IL-1β levels by immunoblotting and amyloid deposition by immunohistochemical staining in brain slices. NLRP1 siRNA treatment did not show a significant change in the expression of active IL-1β (Figure 3f) or the numbers of amyloid plaques (Figures 3g and h) in the brain of APP/PS1 mice.

NLRP1 silencing rescued early cognitive impairment in APPswe/PS1dE9 mice. Because the progressive dysfunction and death of neurons provides a molecular and cellular basis for memory deficits and neuropathological features of dementia in AD,[33] we further investigated the role of NLRP1 in cognitive deficits in APPswe/PS1dE9 mice. Our study demonstrated that the APP/PS1 mice showed impaired spatial learning and memory compared with wild-type mice, as assessed by the Morris water maze (MWM) test. These mice were impaired in learning to use the available spatial cues to locate the submerged escape platform. In contrast, NLRP1 siRNA treatment significantly improved spatial learning as shown by a progressive decrease in time or distance to reach the hidden-platform across consecutive trials (Figures 4a and b). Then, a probe trial was conducted to assess the spatial memory in these mice. APP/PS1 mice failed to spend significantly more time in the target quadrant (Q1) than in all other (a.o.) quadrants, while NLRP1 siRNA treatment has markedly increased time in the target quadrant (Figure 4c). There was no difference in swimming speed or path length among the groups (Figures 4d and e), which enabled us to exclude the effect of motivational factors on mice cognitive performance. In addition, a visual cued testing was performed to discriminate for specific deficits of spatial learning, since—except for the spatial component—cued learning requires similar basic abilities, strategies, and escape motivation. All mice were able to swim directly to the visual platform, and no significant group differences in performance remained (Supplementary Figure S4). All these data suggest that NLRP1 silencing improves spatial cognitive abilities in APPswe/PS1dE9 mice.

Caspase-1 silencing alleviated pyroptosis and cognitive deficits in APPswe/PS1dE9 mice. Considering the central

Figure 3 NLRP1 silencing attenuated neuronal pyroptosis in the APPswe/PS1dE9 brain. Results from 6.5-month-old wild-type (WT) mice and 6.5-month-old APP/PS1 mice after 6 weeks of treatment with the siRNA using a miniosmotic pump. (**a**) Nissl staining was used to observe neuronal morphology and quantify Nissl-positive cell densities in the cerebral cortex and hippocampus of WT mice and APP/PS1 mice. Representative photos were shown. Scale bars: 20 μm. (**b**) Comparison of the Nissl-positive cell densities among the experimental groups. Data are shown as mean ± S.E.M. obtained from six male mice per group. *$P<0.05$, compared with the group of APP/PS1 mice treated with control siRNA. (**c**) Neuronal pyroptosis was detected using the TUNEL staining assay in the cerebral cortex and hippocampus of WT mice and APP/PS1 mice. Neurons with deep black nuclei were identified as TUNEL-positive neurons. Scale bars: 20 μm. (**d**) Comparison of the percentage of TUNEL-positive cells among the experimental groups. Data are shown as mean ± S.E.M. obtained from six male mice per group. *$P<0.05$, compared with the group of APP/PS1 mice treated with control siRNA. (**e**) The expression level of caspase-1 (procaspase-1 p45 45 kD and cleaved caspase-1 p20 subunit 20 kD) was analyzed using the western blot assay. A representative immunoblot is shown, and bands of activated caspase-1 p20 were quantified by densitometry, normalized to β-actin. Data are shown as mean ± S.E.M. obtained from six male mice per group. *$P<0.05$, compared with the group of APP/PS1 mice treated with control siRNA. (**f**) The expression level of cleaved IL-1β (p17) was detected by western blot analysis and quantified by densitometric measurement. β-Actin was used as a loading control. Data are shown as mean ± S.E.M. obtained from six male mice per group. NS, not significant. (**g**) Represent photo of amyloid plaques in cortex and hippocampus of WT mice and APP/PS1 mice treated with control siRNA or NLRP1 siRNA. Amyloid plaques were detected by immunohistochemistry using an antibody against $A\beta_{42}$. The plaques were visualized by microscopy with $\times$200 magnification. Scale bars: 100 μm. (**h**) Quantitative analysis of amyloid plaques among the experimental groups. Data are shown as mean ± S.E.M. obtained from six male mice per group. NS, not significant

role of caspase-1 in the process of neuron pyroptosis and IL-1β secretion, we also knocked down brain caspase-1 in 5-month APP/PS1 mice by *in vivo* non-viral RNA interference methodology for 6 weeks (Supplementary Figures S3c and d). We assessed spatial memory in age-matched mice using the MWM test including probe trial testing. As expected, control siRNA-treated APP/PS1 mice showed severe behavioral deficits in MWM test. However, caspase-1 siRNA treatment could largely improve spatial learning and memory by shortening the time/distance to platform and increasing the time of entrance into the target quadrant (Q1) in APP/PS1 mice (Figures 5a and b; Supplementary Figures S5–S7). Furthermore, the improved cognitive performance after caspase-1 silencing was accompanied by a marked

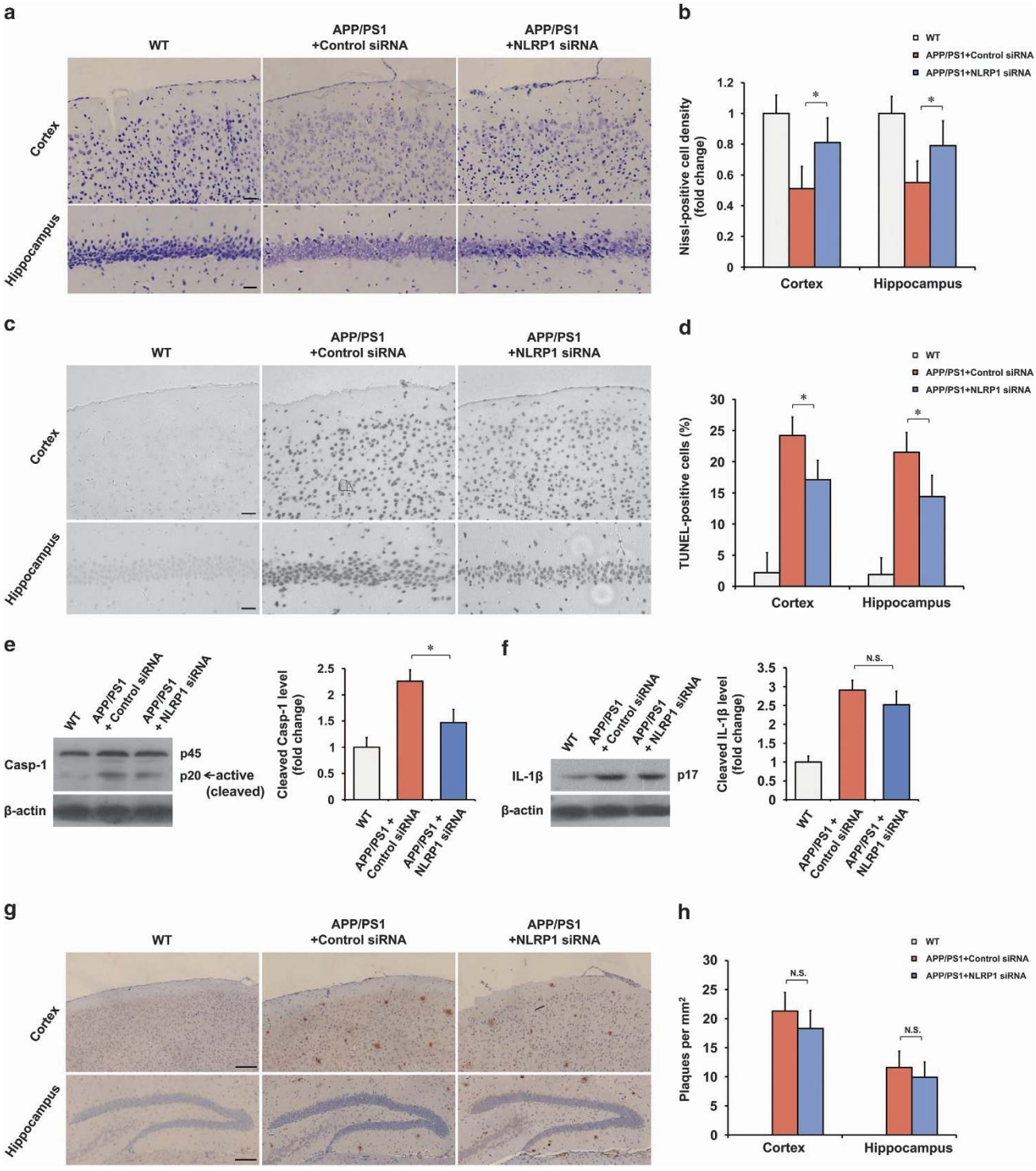

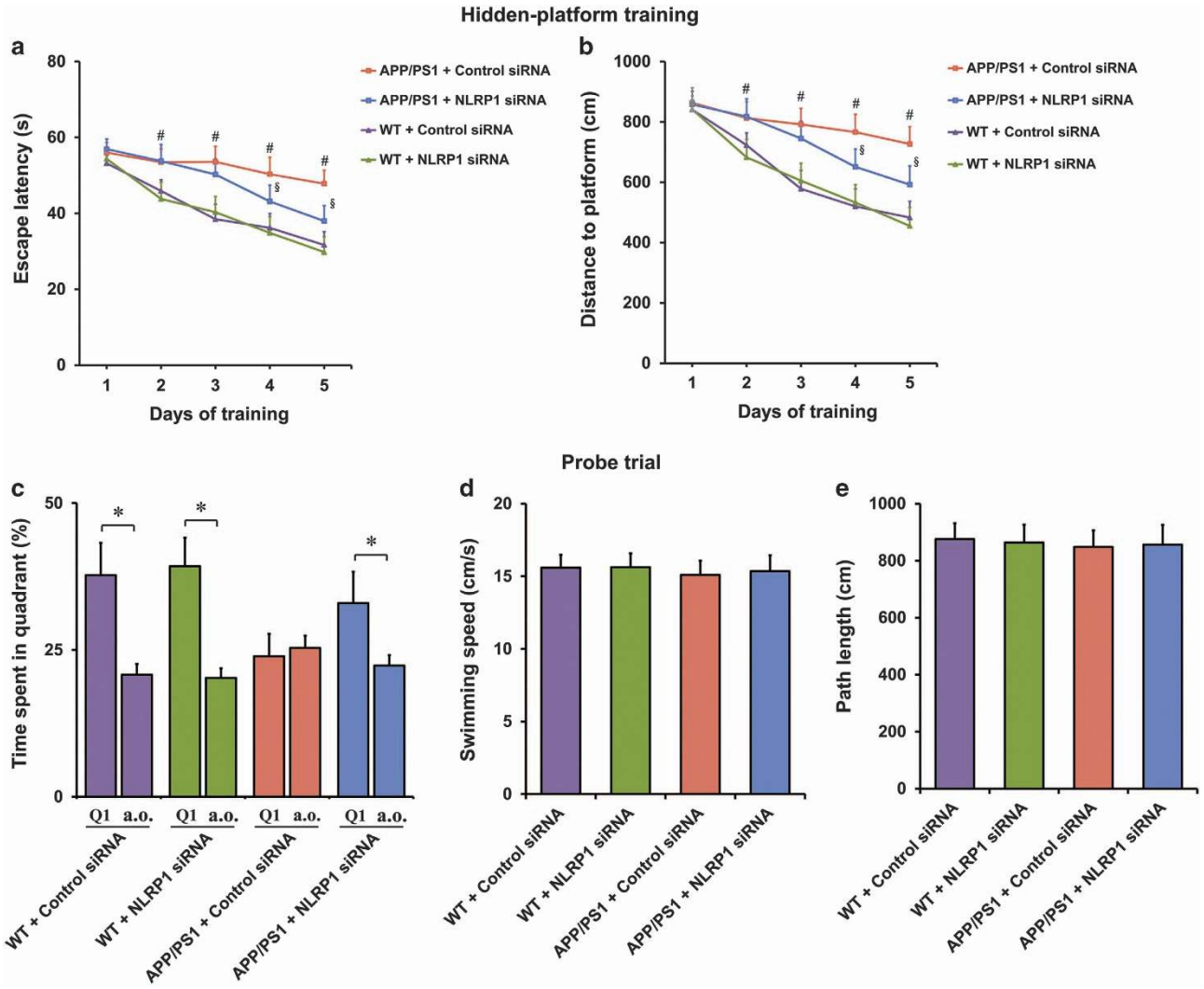

Figure 4 NLRP1 silencing rescued early cognitive deficits in APPswe/PS1dE9 mice. Results from 6.5-month-old wild-type (WT) and APP/PS1 mice after 6 weeks of treatment with NLRP1 siRNA or control siRNA using a miniosmotic pump. During the last 6 days of the treatment, Morris water maze test was conducted to assess the cognitive functions of mice. The Morris water maze test consists of a hidden-platform training last for 5 consecutive days, plus a probe trial conducted at 24 h after the hidden-platform trial. (**a** and **b**) Time to platform (escape latency) and distance to platform of each group in the hidden-platform training. Data were analyzed by two-way repeated-measures ANOVA. $^{\#}P<0.05$ *versus* WT mice treated with control siRNA. $^{\S}P<0.05$ *versus* APP/PS1 mice treated with control siRNA. (**c**) Data from probe trials are presented as percentage of time spent in the target quadrant (Q1) *versus* the averaged time spent in all other (a.o.) quadrants. Q1, quadrant where platform was located on days 1–5. Data were analyzed by independent sample *t*-test. $^{*}P<0.05$ *versus* averaged time spent in a.o. quadrants. (**d** and **e**) To exclude differences in motor performance between groups, swimming speed and path length were recorded and analyzed by a computer-controlled tracking system. Statistical analysis did not reveal any significant differences between groups. Each value represents the mean ± S.E.M. from 18 male mice per group

reduction in TUNEL-positive cell densities and an increase in Nissl-positive cell densities in the cortex and hippocampus of APP/PS1 mice (Figures 5c and d; Supplementary Figure S8). These results are very similar to the changes in NLRP1 siRNA-treated APP/PS1 mice, supporting that NLRP1 acts through caspase-1 to exert the observed effects. In addition, the expression of active IL-1β showed a decrease in the caspase-1 siRNA-treated APP/PS1 brain (Figure 5e). It was noticeable that caspase-1 is a common pathway by which inflammasomes contribute to downstream effects. NLRP3 inflammasome also can activate caspase-1 to induce IL-1β secretion.[4,7] However, our results shown that NLRP3 silencing in APP/PS1 mice brain had no significant effect on TUNEL-positive cell densities in the cortex and hippocampus of APP/PS1 mice (Supplementary Figures S9 and S10). These data further suggest that NLRP1 signaling pathway is essential for the pyroptotic cell death in AD pathogenesis.

Discussion

Recently, the NLRP1 inflammasome has been implicated as a required component in the mechanism underlying pyroptotic cell death.[17,34] A previous study has reported that NLRP1 is highly expressed in the brain, in particular in pyramidal neurons and oligodendrocytes.[16] Moreover, the overexpression of NLRP1 induces neuronal death.[35] Because the neuronal dysfunction and death induced by Aβ, a hallmark of AD that has been believed to play a critical role in the

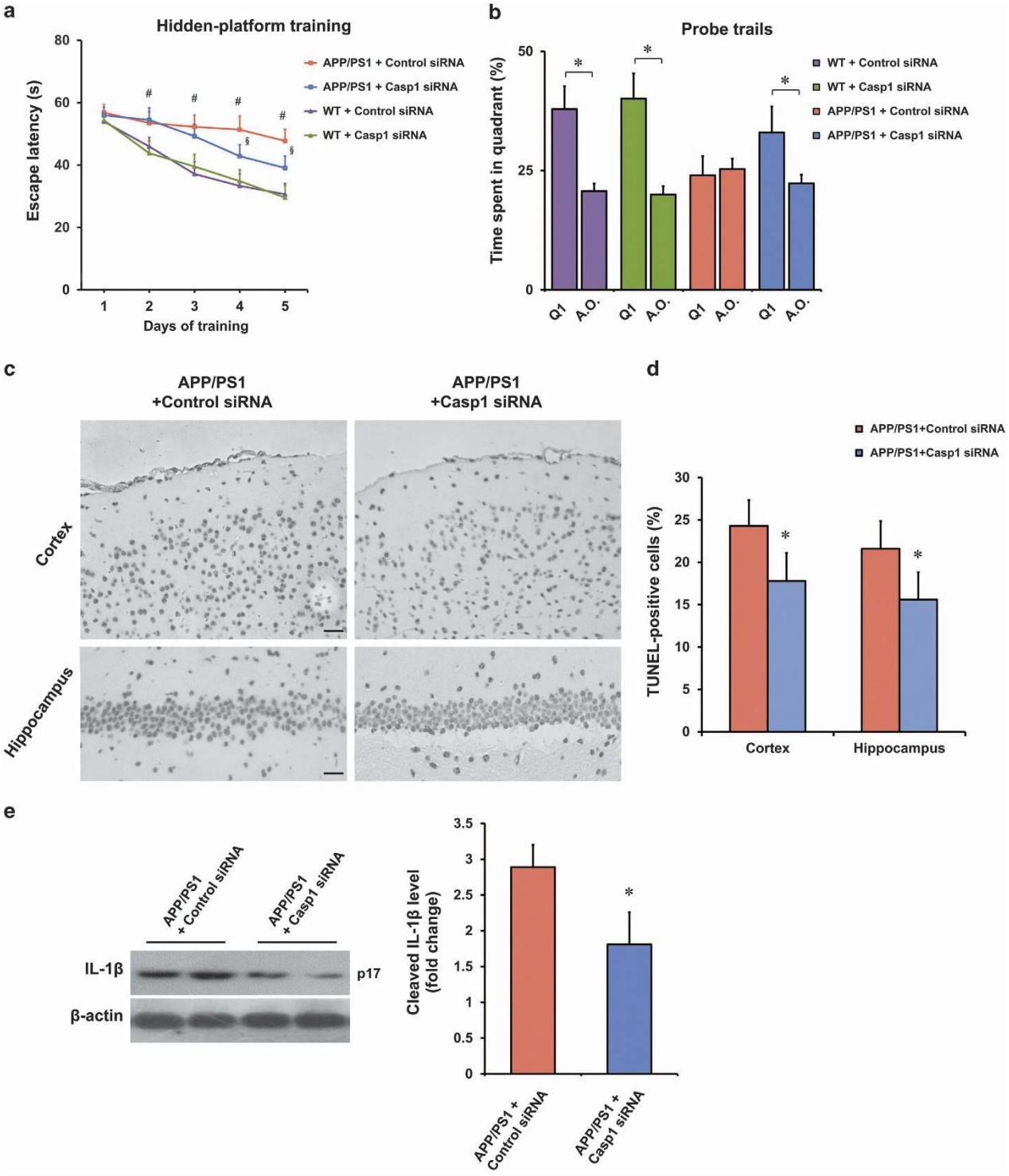

Figure 5 Caspase-1 silencing ameliorated neuronal pyroptosis and cognitive deficits in APPswe/PS1dE9 mice. Data from 6.5-month-old APP/PS1 and wild-type (WT) mice after 6 weeks of treatment with caspase-1 siRNA or control siRNA using a miniosmotic pump. The results of behavioral tests were assessed during last 6 days of siRNA treatment period. (**a**) Escape latency of each group in the hidden-platform training of Morris water maze. Data were analyzed by two-way repeated-measures ANOVA. $^{\#}P<0.05$ *versus* WT mice treated with control siRNA. $^{\S}P<0.05$ *versus* APP/PS1 mice treated with control siRNA. (**b**) Data from probe trials are presented as percentage of time spent in the target quadrant (Q1) *versus* the averaged time spent in all other (a.o.) quadrants. Data were analyzed by independent sample *t*-test. $^{*}P<0.05$ *versus* averaged time spent in a.o. quadrants. After behavioral testing, the caspase-1 siRNA or control siRNA-treated APP/PS1 mice were killed for the following biochemical assays. (**c**) Neuronal pyroptosis was detected using the TUNEL staining assay in the cerebral cortex and hippocampus of siRNA-treated APP/PS1 mice. Neurons with deep black nuclei were identified as TUNEL-positive neurons. Scale bars: 20 μm. (**d**) Quantitative analysis of the percentage of TUNEL-positive cells among the experimental groups. $^{*}P<0.05$ *versus* control siRNA-treated group. (**e**) Western blot analysis of cleaved IL-1β (p17) in brain tissues and densitometrical quantification. β-Actin was used as a loading control. $^{*}P<0.05$ *versus* control siRNA-treated group. All data are shown as mean ± S.E.M. For behavioral testing, $n=18$ male mice per group. For biochemical analyses, $n=6$ male mice per group

cognitive deficits that occurs in AD,[33] we hypothesized that NLRP1-dependent pyroptosis might be a mechanism in AD pathogenesis.

Our study investigated the effects of Aβ-induced NLRP1 on neuronal pyroptosis in *in vitro* model and in APPswe/PS1dE9 mice. We found that the NLRP1 levels were upregulated in the brains of 6- and 9-month-old APP/PS1 mice compared with that in the brains of age-matched wild-type mice. In APPswe/PS1dE9 mice, Aβ accumulation occurs at an early stage; amyloid plaques are visible by 6 months of age,[22] and their content gradually increases with age. Therefore, we considered that the increase in NLRP1 levels was due to Aβ accumulation, and we found that the treatment with $A\beta_{1-42}$ significantly increased the NLRP1 mRNA and protein levels in cultured rat cortical neurons. This finding was consistent with the previous data, in which toxic Aβ peptide may activate the NLRP1 inflammasome via potassium (K^+) efflux.[36,37] These studies have shown that Aβ oligomers can interfere with many aspects of neuronal membrane functions and can evoke K^+ efflux from neurons.[37,38] A low K^+ concentration is a potent activator for the NLRP1 inflammasome.[39] In rat cerebellar granule neurons, withdrawal of serum/K^+ from medium could highly increase the expression of NLRP1.[40]

In this study, we further examined the effect of NLRP1 on neuronal pyroptosis induced by $A\beta_{1-42}$ in cultured cortical neurons, and found that the knockdown of NLRP1 by NLRP1 siRNA transfection significantly reduced the extent of cell death induced by $A\beta_{1-42}$. In addition, the knockdown of NLRP1 attenuated the activation of caspase-1, the secretion of IL-1β and the release of LDH in the Aβ-treated neurons. Since this form of cell death is associated with caspase-1 activation in response to ASC adapter protein oligomerization, plasma membrane permeabilization, and secretion of inflammatory cytokine IL-1β, we refer to this caspase-1-dependent inflammatory form of cell death as pyroptosis.[11] Pyroptosis, a cell death mechanism that is distinct from apoptosis or others.[12] Pyroptosis is triggered by caspase-1 after its activation by various inflammasomes and results in cellular lysis and early release of the cytosolic contents to the extracellular space, including cytosolic proteins such as LDH. This event is predicted to be inherently inflammatory and coincides with IL-1β secretion. Meanwhile, inflammasomes require the adapter protein ASC for the activation of caspase-1.[12] After inflammasome activation, ASC assembles into a large protein complex, which is termed as 'speck' or 'foci'. Hence, ASC speck formation can be used as a simple upstream readout for inflammasome activation; and this has been observed in the Aβ-treated neurons. All these findings above suggested that NLRP1 silencing may protect against Aβ neurotoxicity through caspase-1-dependent pyroptosis mechanism in cultured neuron.

Moreover, this pyroptotic effect of NLRP1 was further confirmed in APPswe/PS1dE9 transgenic mice. Mutations of the *APP* and *PS1* genes have been regarded as one of the causes of familial forms of AD.[41] The APPswe/PS1dE9 mouse, which is associated with familial forms of AD, has been used as an animal model to study the pathogenesis of AD and to explore therapeutic strategies for this disease. These double transgenic mice develop Aβ deposits in the cerebral cortex and the hippocampus much earlier than age-matched mice expressing the *APP* mutation alone.[42] In this study, we found that the APPswe/PS1dE9 mice displayed a significant increase in the number of TUNEL-positive cells and a decrease in Nissl-positive cell densities at 6.5 months of age. These results are consistent with previous findings, in which the early appearance of Aβ deposition in the APP/PS1 mouse brain developed neuronal loss.[43]

To examine the effect of upregulated NLRP1 levels at an early stage in APP/PS1 mice, we performed implantation of miniosmotic pumps for direct infusion of siRNA to knockdown brain NLRP1 expression, starting at 5 months old of age and lasting for 6 weeks until 6.5 months old of age. This RNA interference technology has emerged as a potentially superior alternative to the traditional approaches for assessing gene function in adult animals.[44] Interestingly, application of the non-viral infusion of siRNA into the ventricular system could achieve a widespread sequence-specific gene knockdown in the brain.[25] On the basis of the characteristics of rapid, inexpensive, and specific knockdown of target genes in the whole brain, therefore, this method would accelerate the functional investigation of broadly expressed target genes implicated in neurological disorders. Our study using this approach of pump-mediated siRNA infusion is efficient in downregulation of NLRP1 mRNA (by about 60%) and protein (by about 50%) levels in APP/PS1 brain. And the treatment with control siRNA did not alter cerebral NLRP1 mRNA and protein levels compared with No siRNA-treated APP/PS1 mice, excluding an effect of pump-mediated infusion on NLRP1 expression levels. Similarly, we also knocked down brain caspase-1 by this *in vivo* non-viral RNA interference methodology in 5-month APP/PS1 mice for 6 weeks.

Using the pump-mediated *in vivo* infusion of siRNA in APP/PS1 brain, our study demonstrated that NLRP1 siRNA treatment could significantly reduce TUNEL-positive cell densities and the active caspase-1 expression levels, accompanied by markedly improved spatial learning and memory in APP/PS1 mice. These results support a fundamental role for NLRP1-mediated pyroptosis in behavioral and cognitive dysfunction in AD pathogenesis. Meanwhile, we also knocked down caspase-1 in APP/PS1 brain, and similarly biochemical and behavioral improvements were found between caspase-1 siRNA and NLRP1 siRNA-treated APP/PS1 mice, supporting that NLRP1 acts through caspase-1 to exert the observed effects of pyroptosis and cognitive impairment.

In addition to pyroptosis, NLRP1 inflammasome is responsible for caspase-1-dependent processing of the key pro-inflammatory cytokine IL-1β to an active secreted form.[28,29] And inflammatory mechanisms are also pathogenetic forces in AD. Previous studies have demonstrated that IL-1β is chronically upregulated in AD and believed to serve as a part of inflammatory cycle that regulates AD pathology.[30–32] Although a downward trend of active IL-1β was observed after NLRP1 silencing in APPswe/PS1dE9 brain, this did not reach statistical significance in our current study. This hints to the possibility that NLRP1/caspase-1 signaling pathway is not the only source of IL-1β in the whole brain. While caspase-1 silencing could decrease active IL-1β expression in APP/PS1 brain.

Caspase-1, widely expressed in brain, is a critical pathway by which inflammasomes contribute to downstream effects.

NLRP3 inflammasome also can activate caspase-1 to induce IL-1β secretion.[8] Aβ activated NLRP3 inflammasome is mainly expressed in microglia, which in turn maybe essential for the secretion of pro-inflammatory cytokines and subsequent inflammatory events. Considering that Aβ activated NLRP1 is mainly expressed in neurons, but not in microglial cells,[16] we have reason to infer that the NLRP1 signaling might be more essential for the pyroptotic cell death, a process closely associated with caspase-1 activation and inflammatory cytokine IL-1β secretion. And previous studies have demonstrated that inflammasomes expressed in neurons are involved in the maturation of IL-1β in the central nervous system.[45–47]

Our findings may have clinical implications. Current treatments for AD only have moderate efficacy in improving cognition in patients and do not prevent progression of the disease.[48] Thus, one alternative strategy for achieving neuroprotection may be the inhibition of neuronal pyroptosis. In addition, because AD is a multifactorial disease with complicated pathogenesis, developing multiple targets for treatment might be a new therapeutic strategy.[49] Considering that inhibition of NLRP1 inflammasome had several beneficial effects on neuronal pyroptosis and inflammation response in AD process, modulation of NLRP1 inflammasome may be explored as a promising strategy for the development of AD therapy.

In conclusion, the present study demonstrates that cerebral expression of NLRP1 was upregulated in APP/PS1 mice. The increase in NLRP1 levels in neurons was induced by Aβ, which in turn activated caspase-1 signaling responsible for neuronal pyroptosis and inflammation cytokine release (Figure 6). Using the pump-mediated *in vivo* infusion of non-viral siRNA to knockdown NLRP1 or caspase-1 in the brain of APP/PS1 mice, our study indicated that inhibition of NLRP1 inflammasome represents a promising strategy for the treatment of AD. In view of the differences that are known to exist between human NLRP1 and its murine orthologs,[50] future studies targeting the specific form in mice and application of the findings from animal model to human trials are required to determine the validity of all the hypotheses.

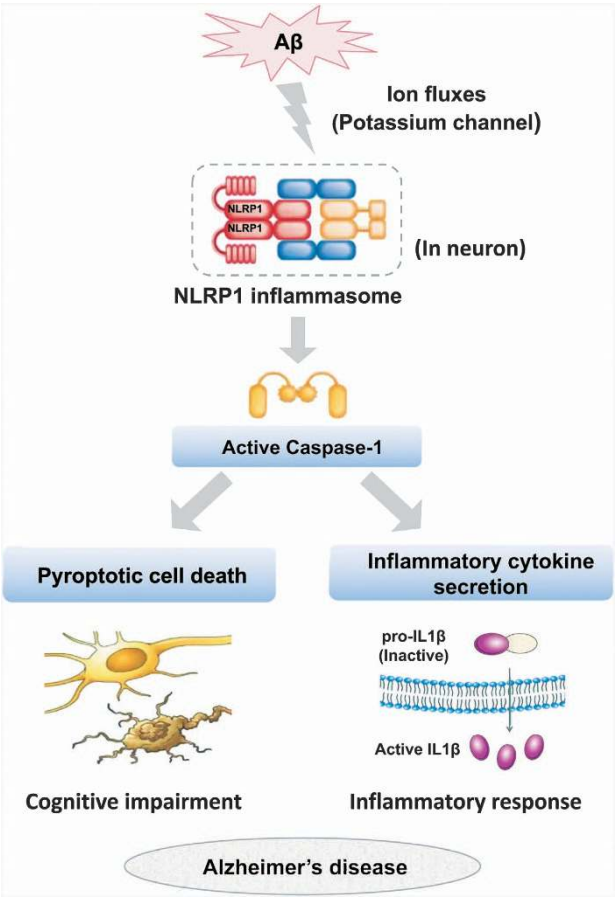

Figure 6 Schematic model linking the NLRP1 inflammasome activation to AD pathogenesis. High NLRP1 levels were found in pyramidal neurons of the brain. The toxic Aβ peptide can set fire to neuronal NLRP1 inflammasome via potassium efflux. Then, the activation of NLRP1 inflammasome leads to the caspase-1-mediated pyroptosis and secretion of IL-1β, which ultimately induces AD pathology through several downstream effects in brain. Our current study mainly indicated that the caspase-1-induced neuronal pyroptosis provides a molecular basis for cognitive deficits in AD process

Materials and Methods

Mice. Male APPswe/PS1dE9 double transgenic mice (B6.Cg-Tg(APPswe, PSEN1dE9)85Dbo/Mmjax) and their age- and background-matched wild-type (WT) mice were purchased from the Model Animal Research Center of Nanjing University. All mouse strains were housed and bred in pathogen-free conditions. The experimental protocol was approved by the Nanjing Medical University Experimental Animal Care and Use Committee. All efforts were made to minimize the number of animals used and their sufferings.

Cell cultures and siRNA transfection. Primary cortical neurons were prepared from Sprague-Dawley rats. Briefly, cerebral cortices from 10 to 12 fetal rats were dissected out, minced, and incubated in 0.25% Trypsin-EDTA (Life Technologies, Carlsbad, CA, USA) at 37 °C for 10 min. The fragments were then dissociated into single cells by pipetting. The dissociated cells were suspended in Neurobasal medium supplemented with 2% B27 (Invitrogen, Carlsbad, CA, USA) and plated onto poly-D-lysine coated 60 mm dishes at a density of 1×10^6/ml. These cells were used on day 4 of plating for further experiments. For siRNA transfection, control siRNA (Santa Cruz Biotechnology, Santa Cruz, CA, USA) and NLRP1 siRNA (Santa Cruz Biotechnology) were transfected into target cells by using Lipofectamine RNAiMAX Reagent (Invitrogen) according to the manufacturer's protocol. The knockdown efficiency was determined at 48 h after transfection by western blotting.

Aβ preparation. The dried synthetic Aβ_{1-42} peptide (Sigma-Aldrich, St. Louis, MO, USA) was first dissolved in dimethylsulfoxide (DMSO), and then diluted in phosphate buffer solution (PBS) to obtain a 250-μM stock solution. This solution was incubated at 4°C for at least 24 h and stored at −80°C until use. Before use, the solution was centrifuged at 12 000 × *g* for 10 min and the supernatant was used as an oligomeric Aβ. The Aβ preparation was evaluated by neurotoxicity and western blotting analysis, and then diluted to a working concentration for further experiments. Reverse sequence peptide Aβ_{42-1} prepared in the same way was used as controls.

Cell viability and cytotoxicity assays. Cell viability was determined using a commercial MTT-based cytotoxicology test kit (Sigma-Aldrich), which detects viable cells colorimetrically based on the detection of the purple formazan compound produced by viable cells. Cells were initially seeded in 96-well plates for 24 h. Forty-eight hours after siRNA transfection, the cells were then incubated in the presence or absence of 5 μM Aβ_{1-42} for 24 h as described above. After removing the supernatant of each well and washing twice by PBS, 20 μl of MTT solution (5 mg/ml in PBS) was added and the culture was further incubated for 4 h. Then, the culture medium was replaced with 100 μl of MTT solubilization solution. The absorbance at 570 nm was measured using a microplate reader (Bio-Rad, Hercules, CA, USA). All treated samples and controls were tested in triplicate.

Cytotoxicity was determined by measuring the release of LDH using the CytoTox One Homogeneous Membrane Integrity Assay (Promega, Madison, WI, USA). The percentage of LDH release was normalized to the condition with the least amount of cell death and divided by a maximum lysis control.

ELISA. Cell culture supernatants were collected and centrifuged at 10 000 × *g*, 4°C for 5 min to remove cell debris. Levels of secreted IL-1β in cell culture supernatants were measured using commercially available ELISA kit (R&D Systems, Minneapolis, MN, USA) according to the manufacturer's instructions.

Immunofluorescence staining. Cells were initially seeded in 96-well plates for 24 h, and then incubated in the presence or absence of 5 μM $A\beta_{1-42}$ for 24 h as described above. After removing the supernatant of each well and washing twice by PBS, cells were fixed, permeabilized with 0.1% Triton X-100, and labeled with DAPI (4′,6-diamidino-2-phenylindole) and anti-ASC antibodies (Calbiochem, La Jolla, CA, USA). Images were taken with the Leica confocal microscope (Leica Microsystems, Wetzlar, Germany).

siRNA administration in mice brain. The NLRP1 siRNA, caspase-1 siRNA, NLRP3 siRNA, and control siRNA were purchased from Santa Cruz Biotechnology, Inc. Entranster-*in vivo* transfection reagent was purchased from Engreen Biosystem Co, Ltd (Beijing, China). The Entranster-*in vivo*–siRNA mixture was prepared in the light of the manufacturer's instructions as previously described.[51,52] Briefly, 12.5 μg siRNA was dissolved in 25 μl RNase-free water. Next, 25 μl siRNA solution was mixed with 25 μl Entranster-*in vivo* transfection reagent and 50 μl artificial cerebrospinal fluid (aCSF, composition in mmol/l: NaCl 130, KCl 2.99, $CaCl_2$ 0.98, $MgCl_2 \bullet 6H_2O$ 0.80, $NaHCO_3$ 25, $N_{a2}HPO_4 \bullet 12H_2O$ 0.039, $NaH_2PO_4 \bullet 2H_2O$ 0.46) to get a 100-μl *in vivo* transfection mixture. This dose of NLRP1 siRNA, caspase-1 siRNA or NLRP3 siRNA infusion was well tolerated, and no signs of neurotoxicity including hind-limb paralysis, vocalization, food intake, or neuroanatomical damage were observed in preliminary study.

We performed implantation of miniosmotic pumps (ALZET) for *in vivo* delivery. After 4 weeks of treatment, we exchanged the old pump reservoir with a new one that was reconnected to the tubing without altering the brain infusion cannula. Briefly, mice were anesthetized with 10% chloral hydrate (0.3 ml/100 g, i.p.) and placed in a stereotactic frame (David Kopf Instrument Inc., Tujunga, CA, USA). A brain-infusion cannula (Brain Infusion Kit 3; ALZET, Cupertino, CA, USA) coupled via vinyl tubing to the osmotic pump was implanted into the dorsal third ventricle (0.5 mm posterior to bregma, 3 mm below the surface of the cranium). The siRNA transfection complex (containing NLRP1, caspase-1 or NLRP3 siRNA, control siRNA, and No siRNA (aCSF only)) was continuously infused into the ventricular system at a flow rate of 0.11 μl/h for 6 weeks by the osmotic pumps. Incidentally, the behavioral and biochemical data between control siRNA-treated and No siRNA-treated mice do not differ.

MWM test. The MWM was conducted during last 6 days of treatment period. It was performed in a circular pool with a diameter of 120 cm filled with opaque water at temperature of 22 ± 1°C, as described previously.[53] In the hidden-platform training, a circular platform (10 cm in diameter) in south-east quadrant was submerged 0.5 cm below the surface of water. Mice were allowed to search for the platform for 60 s; if a mouse failed to find the platform within 60 s, it was picked up and placed on the platform for 15 s. All mice were given four training trials per day for 5 consecutive days. Twenty-four hours after the hidden-platform trial, mice were subjected to a probe trial in which the platform was removed, and their swimming paths were recorded for 60 s. Then, a visual cued testing was performed with the platform being flagged and blank curtains are closed around the pool to avoid access to distal visual cues. To ensure that mice are using the visual cue to locate the platform, both the location of the goal and the starting point are moved to new positions during each trial. All mice behavior (time/distance for reaching the platform, swimming speed, path length, and time spent in each quadrant) was monitored by a video camera and analyzed by a computer-controlled system (Beijing Sunny Instruments Inc., Beijing, China).

Brain tissue preparation. After the treatment with siRNA in the brain using a miniosmotic pump, behavioral testing was conducted, and then, mice were killed for the following biochemical assays. After perfusion, the brains were rapidly isolated and placed on an ice-cooled cutting board; hippocampus and cortex were removed from one hemisphere and snap-frozen until subject to RNA or protein extraction. For the immunohistochemistry assay, the other hemisphere was placed in 4% paraformaldehyde in PBS (pH 7.4) overnight.

Real-time PCR. Total RNA was extracted from the cells and brain tissue using the Trizol reagent (Invitrogen) according to the manufacturer's protocol. Samples (1 μg of RNA) were reverse-transcribed into cDNA using the Prime-Script one step RT reagent Kit (TaKaRa, Madison, WI, USA). Synthesized cDNA was used in real-time PCR experiments using the SYBR Premix Ex Taq (TaKaRa), and then analyzed with CFX96 Real-Time PCR detection system (Bio-Rad). All reactions were run in duplicates and the mean values are used. The relative expression of each mRNA was calculated using the comparative $2^{-\Delta\Delta Ct}$ method and was normalized against glyceraldehyde-3-phosphate dehydrogenase (GAPDH). Primers were purchased from Invitrogen as follows (name: forward primer, reverse primer): rat *nlrp1*: 5′-gccctggagacaaagaatcc-3′, 5′-agtgggcatcgtcatgtgt-3′; rat *caspase-1*: 5′-aaggtcctgagggcaaagag-3′, 5′-gtgttgcagataatgagggc-3′; rat *gapdh*: 5′-cagtgccagcctcgtctcat-3′, 5′-aggggccatccacagtcttc-3′; mouse *nlrp1*: 5′-tggcacatcctagggaaatc-3′, 5′-tcctcacgtgacagcagaac-3′; mouse *caspase-1*: 5′-tc cgcggttgaatccttttcaga-3′, 5′-accacaattgctgtgtgtgcgca-3; mouse *gapdh*: 5′-caacag caactcccactcttc-3′, 5′-ggtccagggtttcttactcctt-3′.

Western blotting. For western blotting, cells as well as brain tissues were lysed in extraction buffer (Beyotime Inc., Shanghai, China) containing complete protease inhibitor cocktail (Roche, Indianapolis, IN, USA). The protein concentrations were determined using the BCA protein assay kit (Beyotime Inc.). Different samples with an equal amount of protein were separated on 10–15% SDS polyacrylamide gels, and transferred onto PVDF membranes. The membranes were blocked with non-fat milk and incubated at 4°C overnight, with the primary antibodies against NLRP1 (1 : 400; Santa Cruz Biotechnology), NeuN (1 : 500; Chemicon, Temecula, CA, USA), Caspase-1 (1 : 500; Abcam, Cambridge, MA, USA), cleaved IL-1β (1 : 500; Santa Cruz Biotechnology), NLRP3 (1 : 500; Santa Cruz Biotechnology), and β-actin (1 : 500; Santa Cruz Biotechnology). After rinsing, the membranes were appropriately incubated with horseradish peroxidase (HRP)-conjugated suitable secondary antibodies (1 : 5000; Zhongshan Inc., Beijing, China) for 2 h at room temperature. After washing, protein bands were detected with a chemiluminescent HRP substrate (Thermo Scientific, Waltham, MA, USA) for 5 min at room temperature and exposed to X-ray film (Fujifilm). The signal intensity was analyzed using the Quantity One software 4.6.2 (Bio-Rad) and normalized to the loading control β-actin. Incidentally, there are three orthologs of NLRP1 (Nlrp1a-c) exist in mice, and the NLRP1 antibody used in our experiment could detect Nlrp1a, Nlrp1b, and Nlrp1c of mouse and rat origin. To ensure the specificity of the immunoblotting procedure, control experiments were performed in which the corresponding primary antibody was omitted. Under these conditions, no signal was observed.

Immunohistochemistry analysis. The brains were embedded in paraffin and cut into 4–6 μm sections. For immunohistochemistry analysis, the sections were immersed in 3% H_2O_2 for 30 min to block endogenous peroxidase activity. After being washed in PBS, the sections were blocked with 5% BSA for 30 min, incubated with a rabbit polyclonal antibody against $A\beta_{42}$ (1 : 600; Abcam) overnight at 4°C, and then treated with appropriate biotinylated secondary antibody (Zhongshan Inc.) for 60 min. Immunoreactivity was detected with diaminobenzidine. Finally, sections were then counterstained with Mayer's hematoxylin (Sigma-Aldrich), dehydrated, mounted on the slides and examined with a microscope equipped with a charge-coupled device camera. Quantification of amyloid plaques was assessed by measuring the Aβ-immunostained area of cortical and hippocampal regions on the section. We performed analysis of six defined regions per mouse brain and the mean count was recorded for each mouse.

For double immunofluorescence staining, the sections were blocked with 5% BSA and 0.1% Triton X-100 for 2 h at room temperature. After a single wash with PBS, sections were incubated overnight at 4°C with a rabbit polyclonal antibody against NLRP1 (1 : 100; Santa Cruz Biotechnology), as well as a mouse monoclonal antibody against NeuN (1 : 200; Chemicon). Sections were then washed in PBS and sequentially incubated respectively with FITC-conjugated anti-rabbit IgG (1 : 200; Zhongshan Inc.) and TRITC-conjugated anti-mouse IgG (1 : 200; Zhongshan Inc.) in a dark and humidified container for 1 h at 37°C. After that, the sections were washed with PBS and sealed with a coverslip. The slides were analyzed with a fluorescence microscopy (Olympus, BX51, Tokyo, Japan). To ensure the specificity of the double-immunostaining procedure, control experiments were performed in which one of the two primary antibodies or both were omitted. Under these conditions, no staining for NLRP1 or NeuN was observed.

TUNEL assay. For TUNEL assay, a cell death detection kit was used (*In Situ* Cell Death Detection Kit, POD; Roche). The presence of nicks in the DNA of cultured cells was identified by terminal deoxynucleotidyl transferase (TdT), an enzyme that catalyzes the addition of labeling dUTPs. Briefly, cells grown on

12-mm coverslips were fixed in 4% paraformaldehyde for 10 min at room temperature and then rinsed in PBS. Cells were then permeabilized for 2 min on ice before labeling with 50 μl of TUNEL reaction mixture and incubating for 60 min at 37°C in a humidified chamber under parafilm coverslips. After washing with PBS, slides were mounted in DAPI-containing Vectashield and examined by fluorescence microscopy (Olympus, BX51).

The paraffin-embedded sections of mice brain received deparaffinization and rehydration treatments, and then were incubated with proteinase-K for 15 min at room temperature followed by three washes in PBS. The TUNEL reaction mixture was added and incubated for 60 min at 37°C. Sections were then washed with PBS and had applied two drops of peroxidase-streptavidin conjugate solution in blocking buffer. They were incubated for 30 min at room temperature, washed again with PBS and exposed to 0.03% diaminobenzidine in 0.01% H_2O_2. At the end of this procedure, sections were counterstained with Mayer's hematoxylin, dehydrated, mounted on the slides and examined with a microscope equipped with a charge-coupled device camera. Neurons with deep black nuclei were identified as TUNEL-positive neurons.

Nissl staining. Neuronal morphology in brain sections was evaluated after cresyl violet staining of Nissl bodies. Briefly, after deparaffinage, sections were incubated with cresyl violet solution, destained in 96% ethanol containing 0.5% acetic acid, dehydrated with isopropanol, cleared in xylene and mounted under coverslips. A computer-assisted light microscope (Olympus, BX51) was used to scan the sections. The densities of Nissl-positive cells in the cortex and hippocampus of the scanned digital images were calculated using Image-Pro Express software (Media Cybernetics, Silver Spring, MD, USA). The total cell counts were averaged from six sections per animal.

Statistical analysis. Statistical analysis was conducted by SPSS software 13.0 (SPSS, Inc., Chicago, IL, USA). After confirming normal distribution with skewness and kurtosis statistic test, independent sample *t*-test or one-way ANOVA followed by least significant difference (LSD) *post hoc* test used to analyze differences among groups. All data are expressed as mean ± S.E.M. $P<0.05$ was considered as statistically significant. For the hidden-platform training of the MWM test, time/distance to platform of each group was analyzed by two-way repeated-measures ANOVA with two factors: the groups and the training days (with repeated measures on the second factor). For the two sets of comparisons, both main effects (group and day) and interaction (group *versus* day) were obtained as statistical parametric maps. On all such maps, an effect was considered significant when the statistical threshold was $P<0.05$ (corrected for multiple comparisons using the false discovery rate (FDR) method).[54]

Conflict of Interest

The authors declare no conflict of interest.

Acknowledgements. This work was supported by grants from the National Natural Science Foundation of China (81000544, 81171209 and 81371406), the Shandong Provincial Natural Science Foundation, China (ZR2010HQ004 and ZR2011HZ001), the Medicine and Health Science Technology Development Project of Shandong Province (2011WSA02018 and 2011WSA02020), and the Shandong Provincial Outstanding Medical Academic Professional Program.

Author contributions

MST and JTY designed, performed experiments, analyzed data, and drafted the first draft. TJ, XCZ, and HFW performed and analyzed data. CDJ participated in the experiment design, edited the manuscript. LT designed and supervised experiments.

1. Hardy J, Selkoe DJ. The amyloid hypothesis of Alzheimer's disease: progress and problems on the road to therapeutics. *Science* 2002; **297**: 353–356.
2. Selkoe DJ. Alzheimer's disease: genes, proteins, and therapy. *Physiol Rev* 2001; **81**: 741–766.
3. Parihar MS, Hemnani T. Alzheimer's disease pathogenesis and therapeutic interventions. *J Clin Neurosci* 2004; **11**: 456–467.
4. Heneka MT, Kummer MP, Stutz A, Delekate A, Schwartz S, Vieira-Saecker A *et al.* NLRP3 is activated in Alzheimer's disease and contributes to pathology in APP/PS1 mice. *Nature* 2013; **493**: 674–678.
5. Tan MS, Yu JT, Jiang T, Zhu XC, Tan L. The NLRP3 inflammasome in Alzheimer's disease. *Mol Neurobiol* 2013; **48**: 875–882.
6. Liu L, Chan C. The role of inflammasome in Alzheimer's disease. *Ageing Res Rev* 2014; **15C**: 6–15.
7. Masters SL, O'Neill LA. Disease-associated amyloid and misfolded protein aggregates activate the inflammasome. *Trends Mol Med* 2011; **17**: 276–282.
8. Halle A, Hornung V, Petzold GC, Stewart CR, Monks BG, Reinheckel T *et al.* The NALP3 inflammasome is involved in the innate immune response to amyloid-beta. *Nat Immunol* 2008; **9**: 857–865.
9. Franchi L, Eigenbrod T, Munoz-Planillo R, Nunez G. The inflammasome: a caspase-1-activation platform that regulates immune responses and disease pathogenesis. *Nat Immunol* 2009; **10**: 241–247.
10. Lamkanfi M, Dixit VM. Mechanisms and functions of inflammasomes. *Cell* 2014; **157**: 1013–1022.
11. Bergsbaken T, Fink SL, Cookson BT. Pyroptosis: host cell death and inflammation. *Nat Rev Microbiol* 2009; **7**: 99–109.
12. Miao EA, Rajan JV, Aderem A. Caspase-1-induced pyroptotic cell death. *Immunol Rev* 2011; **243**: 206–214.
13. Sastre M, Richardson JC, Gentleman SM, Brooks DJ. Inflammatory risk factors and pathologies associated with Alzheimer's disease. *Curr Alzheimer Res* 2011; **8**: 132–141.
14. Eikelenboom P, Veerhuis R, van Exel E, Hoozemans JJ, Rozemuller AJ, van Gool WA. The early involvement of the innate immunity in the pathogenesis of late-onset Alzheimer's disease: neuropathological, epidemiological and genetic evidence. *Curr Alzheimer Res* 2011; **8**: 142–150.
15. Krstic D, Madhusudan A, Doehner J, Vogel P, Notter T, Imhof C *et al.* Systemic immune challenges trigger and drive Alzheimer-like neuropathology in mice. *J Neuroinflammation* 2012; **9**: 151.
16. Kummer JA, Broekhuizen R, Everett H, Agostini L, Kuijk L, Martinon F *et al.* Inflammasome components NALP 1 and 3 show distinct but separate expression profiles in human tissues suggesting a site-specific role in the inflammatory response. *J Histochem Cytochem* 2007; **55**: 443–452.
17. Masters SL, Gerlic M, Metcalf D, Preston S, Pellegrini M, O'Donnell JA *et al.* NLRP1 inflammasome activation induces pyroptosis of hematopoietic progenitor cells. *Immunity* 2012; **37**: 1009–1023.
18. de Rivero Vaccari JP, Lotocki G, Alonso OF, Bramlett HM, Dietrich WD, Keane RW. Therapeutic neutralization of the NLRP1 inflammasome reduces the innate immune response and improves histopathology after traumatic brain injury. *J Cereb Blood Flow Metab* 2009; **29**: 1251–1261.
19. Abulafia DP, de Rivero Vaccari JP, Lozano JD, Lotocki G, Keane RW, Dietrich WD. Inhibition of the inflammasome complex reduces the inflammatory response after thromboembolic stroke in mice. *J Cereb Blood Flow Metab* 2009; **29**: 534–544.
20. Mawhinney LJ, de Rivero Vaccari JP, Dale GA, Keane RW, Bramlett HM. Heightened inflammasome activation is linked to age-related cognitive impairment in Fischer 344 rats. *BMC Neurosci* 2011; **12**: 123.
21. Pontillo A, Catamo E, Arosio B, Mari D, Crovella S. NALP1/NLRP1 genetic variants are associated with Alzheimer disease. *Alzheimer Dis Assoc Disord* 2012; **26**: 277–281.
22. Jankowsky JL, Fadale DJ, Anderson J, Xu GM, Gonzales V, Jenkins NA *et al.* Mutant presenilins specifically elevate the levels of the 42 residue beta-amyloid peptide in vivo: evidence for augmentation of a 42-specific gamma secretase. *Hum Mol Genet* 2004; **13**: 159–170.
23. Larson ME, Lesne SE. Soluble Abeta oligomer production and toxicity. *J Neurochem* 2012; **120**(Suppl 1): 125–139.
24. Lambert MP, Viola KL, Chromy BA, Chang L, Morgan TE, Yu J *et al.* Vaccination with soluble Abeta oligomers generates toxicity-neutralizing antibodies. *J Neurochem* 2001; **79**: 595–605.
25. Thakker DR, Natt F, Husken D, Maier R, Muller M, van der Putten H *et al.* Neurochemical and behavioral consequences of widespread gene knockdown in the adult mouse brain by using nonviral RNA interference. *Proc Natl Acad Sci USA* 2004; **101**: 17270–17275.
26. Cryan JF, Thakker DR, Hoyer D. Emerging use of non-viral RNA interference in the brain. *Biochem Soc Trans* 2007; **35**(Pt 2): 411–415.
27. Thakker DR, Hoyer D, Cryan JF. Interfering with the brain: use of RNA interference for understanding the pathophysiology of psychiatric and neurological disorders. *Pharmacol Ther* 2006; **109**: 413–438.
28. Denes A, Lopez-Castejon G, Brough D. Caspase-1: is IL-1 just the tip of the ICEberg? *Cell Death Dis* 2012; **3**: e338.
29. Levandowski CB, Mailloux CM, Ferrara TM, Gowan K, Ben S, Jin Y *et al.* NLRP1 haplotypes associated with vitiligo and autoimmunity increase interleukin-1beta processing via the NLRP1 inflammasome. *Proc Natl Acad Sci USA* 2013; **110**: 2952–2956.
30. Apelt J, Schliebs R. Beta-amyloid-induced glial expression of both pro- and anti-inflammatory cytokines in cerebral cortex of aged transgenic Tg2576 mice with Alzheimer plaque pathology. *Brain Res* 2001; **894**: 21–30.
31. Shaftel SS, Kyrkanides S, Olschowka JA, Miller JN, Johnson RE, O'Banion MK. Sustained hippocampal IL-1 beta overexpression mediates chronic neuroinflammation and ameliorates Alzheimer plaque pathology. *J Clin Invest* 2007; **117**: 1595–1604.
32. Swardfager W, Lanctot K, Rothenburg L, Wong A, Cappell J, Herrmann N. A meta-analysis of cytokines in Alzheimer's disease. *Biol Psychiatry* 2010; **68**: 930–941.
33. Mattson MP. Pathways towards and away from Alzheimer's disease. *Nature* 2004; **430**: 631–639.

34. Kovarova M, Hesker PR, Jania L, Nguyen M, Snouwaert JN, Xiang Z *et al.* NLRP1-dependent pyroptosis leads to acute lung injury and morbidity in mice. *J Immunol* 2012; **189**: 2006–2016.
35. Liu F, Lo CF, Ning X, Kajkowski EM, Jin M, Chiriac C *et al.* Expression of NALP1 in cerebellar granule neurons stimulates apoptosis. *Cell Signal* 2004; **16**: 1013–1021.
36. Salminen A, Ojala J, Suuronen T, Kaarniranta K, Kauppinen A. Amyloid-beta oligomers set fire to inflammasomes and induce Alzheimer's pathology. *J Cell Mol Med* 2008; **12**: 2255–2262.
37. Yu SP, Farhangrazi ZS, Ying HS, Yeh CH, Choi DW. Enhancement of outward potassium current may participate in beta-amyloid peptide-induced cortical neuronal death. *Neurobiol Dis* 1998; **5**: 81–88.
38. Colom LV, Diaz ME, Beers DR, Neely A, Xie WJ, Appel SH. Role of potassium channels in amyloid-induced cell death. *J Neurochem* 1998; **70**: 1925–1934.
39. Petrilli V, Papin S, Dostert C, Mayor A, Martinon F, Tschopp J. Activation of the NALP3 inflammasome is triggered by low intracellular potassium concentration. *Cell Death Differ* 2007; **14**: 1583–1589.
40. Frederick Lo C, Ning X, Gonzales C, Ozenberger BA. Induced expression of death domain genes NALP1 and NALP5 following neuronal injury. *Biochem Biophys Res Commun* 2008; **366**: 664–669.
41. Bertram L, Tanzi RE. Thirty years of Alzheimer's disease genetics: the implications of systematic meta-analyses. *Nat Rev Neurosci* 2008; **9**: 768–778.
42. Kurt MA, Davies DC, Kidd M, Duff K, Rolph SC, Jennings KH *et al.* Neurodegenerative changes associated with beta-amyloid deposition in the brains of mice carrying mutant amyloid precursor protein and mutant presenilin-1 transgenes. *Exp Neurol* 2001; **171**: 59–71.
43. Faure A, Verret L, Bozon B, El Tannir El Tayara N, Ly M, Kober F *et al.* Impaired neurogenesis, neuronal loss, and brain functional deficits in the APPxPS1-Ki mouse model of Alzheimer's disease. *Neurobiol Aging* 2011; **32**: 407–418.
44. Dorsett Y, Tuschl T. siRNAs: applications in functional genomics and potential as therapeutics. *Nat Rev Drug Discov* 2004; **3**: 318–329.
45. Fann DY, Lee SY, Manzanero S, Tang SC, Gelderblom M, Chunduri P *et al.* Intravenous immunoglobulin suppresses NLRP1 and NLRP3 inflammasome-mediated neuronal death in ischemic stroke. *Cell Death Dis* 2013; **4**: e790.
46. Zou J, Crews FT. Inflammasome-IL-1beta signaling mediates ethanol inhibition of hippocampal neurogenesis. *Front Neurosci* 2012; **6**: 77.
47. de Rivero Vaccari JP, Lotocki G, Marcillo AE, Dietrich WD, Keane RW. A molecular platform in neurons regulates inflammation after spinal cord injury. *J Neurosci* 2008; **28**: 3404–3414.
48. Sevilla C, Jimenez Caballero PE, Alfonso V, Gonzalez-Adalid M. Current treatments of Alzheimer disease: are main caregivers satisfied with the drug treatments received by their patients? *Dement Geriatr Cogn Disord* 2009; **28**: 196–205.
49. Youdim MB, Buccafusco JJ. CNS Targets for multi-functional drugs in the treatment of Alzheimer's and Parkinson's diseases. *J Neural Transm* 2005; **112**: 519–537.
50. Sastalla I, Crown D, Masters SL, McKenzie A, Leppla SH, Moayeri M. Transcriptional analysis of the three Nlrp1 paralogs in mice. *BMC Genomics* 2013; **14**: 188.
51. Tan MS, Yu JT, Jiang T, Zhu XC, Guan HS, Tan L. IL12/23 p40 inhibition ameliorates Alzheimer-associated neuropathology and spatial memory in SAMP8 mice. *J Alzheimers Dis* 2014; **38**: 633–646.
52. Jiang T, Yu JT, Zhu XC, Tan MS, Gu LZ, Zhang YD *et al.* Triggering receptor expressed on myeloid cells 2 knockdown exacerbates aging-related neuroinflammation and cognitive deficiency in senescence-accelerated mouse prone 8 mice. *Neurobiol Aging* 2014; **35**: 1243–1251.
53. Vorhees CV, Williams MT. Morris water maze: procedures for assessing spatial and related forms of learning and memory. *Nat Protoc* 2006; **1**: 848–858.
54. Benjamini Y, Hochberg Y. Controlling the false discovery rate: a practical and powerful approach to multiple testing. *J Roy Stat Soc B* 1995; **57**: 289–300.

Supplementary Information accompanies this paper on Cell Death and Disease website (http://www.nature.com/cddis)